AGU100 ADVANCING EARTH AND SPACE SCIENCE

Geophysical Research Letters

RESEARCH LETTER
10.1002/2017GL076583

Key Points:
- Guided wave arrivals resolve low seismic velocities associated with unmetamorphosed crust in the subducted Yakutat terrane
- The subducted terrane is found to be 6 to 10 km thick at intermediate depths, notably thinner than previously suggested
- Thinning of the Yakutat to 50–75%, its initial thickness implies significant underplating and/or metamorphism of upper parts of the terrane

Supporting Information:
- Supporting Information S1

Correspondence to:
S. Coulson,
slcoulson@g.harvard.edu

Citation:
Coulson, S., Garth, T., & Rietbrock, A. (2018). Velocity structure of the subducted Yakutat terrane, Alaska: Insights from guided waves. *Geophysical Research Letters*, *45*, 3420–3428. https://doi.org/10.1002/2017GL076583

Received 28 NOV 2017
Accepted 28 MAR 2018
Accepted article online 2 APR 2018
Published online 16 APR 2018

The copyright line for this article was changed on 7 MAY 2018 after original online publication.

Velocity Structure of the Subducted Yakutat Terrane, Alaska: Insights From Guided Waves

S. Coulson[1,2], T. Garth[1,3], and A. Rietbrock[1,4]

[1]Department of Earth, Ocean and Ecological Sciences, University of Liverpool, Liverpool, UK, [2]Now at Department of Earth and Planetary Sciences, Harvard University, Cambridge, MA, USA, [3]Now at Department of Earth Sciences, University of Oxford, Oxford, UK, [4]Now at Geophysical Institute, Karlsruhe Institute of Technology, Karlsruhe, Germany

Abstract Dispersed *P* wave arrivals from intermediate-depth earthquakes in the Alaskan subduction zone provide insight into the low-velocity structure of the subducting oceanic crust. *P* wave arrivals from 41 earthquakes in the eastern section of the arc show significant guided wave dispersion, with high-frequency (>1 Hz) energy delayed by up to 2–3 s. We simulate this dispersion using a 2-D finite difference waveform propagation model, systematically varying both *P* wave velocity and low-velocity layer thickness parameters to find the lowest misfit between the observed and synthetic waveforms. We infer a 6 to 10 km thick low-velocity layer with a *P* wave velocity contrast of 7–15% with the overriding mantle, velocities which cannot be entirely accounted for by metamorphosed mid-ocean ridge basalt compositions. We postulate that this structure is the remnant of the subducted Yakutat terrane, significantly thinned at depth by metamorphism or delamination of material during subduction.

Plain Language Summary In the Alaskan subduction zone the Pacific plate sinks beneath the North American tectonic plate. As it sinks, deformation and increased temperature and pressure in the Pacific plate cause earthquakes to occur, sometimes as much as 200 km beneath the Earth's surface. These earthquakes, deep within the subduction zone, radiate seismic waves that travel through the subducted crust and are observed at seismic stations across Alaska. We use these signals recorded at the surface to infer the geological structure of the subduction zone. The timing of energy arriving at the seismic stations tells us about the physical structure of the rocks at depth within the subducted Pacific plate. We determine that although the oceanic plate is anomalously thick at Earth's surface, it has been significantly thinned as it has been subducted. Additionally, the crustal rock properties have not changed as much as expected for such high temperature and pressure conditions present deep in the subduction zone. Increasing our understanding of the geological structure, the Alaskan subduction zone is fundamental in understanding the potential for powerful earthquakes in this region.

1. Introduction

Subducting slabs are characterized by a thick, high-velocity layer of slab mantle capped by a low-velocity layer (LVL), thought to be partially metamorphosed subducted crust (e.g., Hacker et al., 2003; Kirby et al., 1996; Martin et al., 2003). LVLs are widely accepted to be present in subduction zones globally down to depths of 150–220 km, where it is thought that the crust becomes fully eclogitized and therefore no longer seismically distinguishable from mantle hazburgite (e.g., Hacker et al., 2003).

Some of the most compelling constraints on the structure of subducted LVLs come from guided wave observations, where the velocity structure is inferred from dispersion of *P* waves arrivals observed from earthquakes within the subducted crust (Abers, 2000, 2005; Garth & Rietbrock, 2014a, 2017; Martin et al., 2003). *P* wave dispersion occurs as high-frequency (>1 Hz), short-wavelength seismic waves propagate through the low-velocity subducted crust, which acts as a waveguide, while lower frequency energy (<1 Hz) travels through the high-velocity surrounding mantle. High-frequency energy then decouples from the low-velocity crustal waveguide and is seen in the forearc creating a delayed high-frequency arrival, approximately 1–4 s after low-frequency arrivals. Delayed high-frequency energy can therefore be used to deduce the seismic properties of the subducted crust. Dispersive arrivals have been used to infer the prevalence of LVL structures in subduction zones across the globe (Abers, 2000, 2005; Martin & Rietbrock, 2006) and have also been shown to be sensitive to low-velocity structure associated with hydrated fault zones in the lithospheric mantle (Garth & Rietbrock, 2014b, 2017).

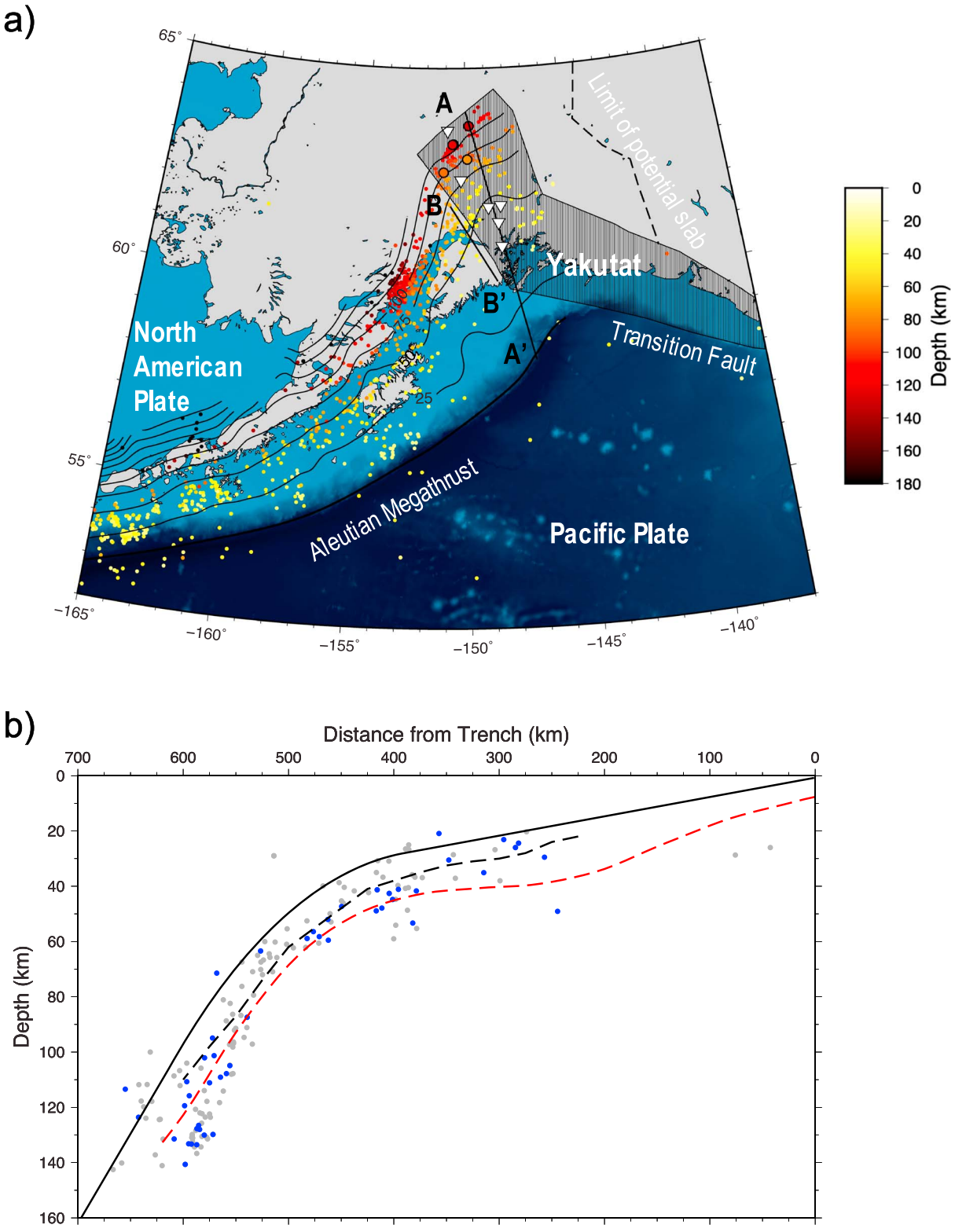

Figure 1. Summary map and profile. (a) Study area in southern Alaska. Preliminary Determination of Epicenters (PDE) catalog from 2010 to 2016 shown in color, with events used in this study highlighted with black outline. Slab1.0 model contours are given at 25 m depth intervals in black (Hayes et al., 2012). AK stations used are shown as white triangles along the line of section A-A′. The line B-B′ is the receiver function cross section of Kim et al. (2014). Inferred extent of the subducting Yakutat microplate is overlaid as a hatched area (Eberhart-Phillips et al., 2006). (b) Profile A in cross sectional view. The grey points show the PDE catalog as above, and the blue points show the well-located International Seismological Centre catalog. Slab1.0 is plotted as a dashed red line, the slab top inferred by Kim et al. (2014) is shown by a dashed black line, and the slab top used for modeling is shown by a solid black line.

In the eastern Alaskan subduction zone presence of an unusually thick LVL associated with the Yakutat terrane has been inferred down to ~140 km depth by receiver functions (Ferris et al., 2003; Kim et al., 2014; Rondenay et al., 2008) and detailed traveltime tomography (Eberhart-Phillips et al., 2006). Low-velocity structure has also been inferred in the area from observations of guided wave dispersion (Abers, 2000, 2005; Abers & Sarker, 1996); however, the along-strike raypaths used mainly sampled the thinner LVL to the west of the Yakutat terrane.

In this paper, we show that high-frequency (>1 Hz) *P* wave arrivals from earthquakes at 70 to 140 km depth, within the region where the Yakutat microplate is subducted, are delayed by up to 2–3 s. Full waveform modeling of the dispersed arrivals provides new constraints on the velocity and width of the anomalously thick LVL associated with the subducting Yakutat terrane.

2. Tectonic Setting and Slab Shape

The Yakutat terrane is believed to be an accreted section of oceanic plateau of 15–30 km thickness, which is overlain by several kilometers of sediment (Christeson et al., 2010; Worthington et al., 2012). The terrane is coupled with the Pacific plate at its western edge, as shown by the black dashed line in Figure 1a, and is seen to be subducting down to ~140 km depth (Kim et al., 2014; Rondenay et al., 2008). The buoyancy of the subducting Yakutat terrane has led to low-angle subduction in eastern Alaska, increasing the area of the megathrust and allowing it to support the second most powerful earthquake ever recorded, the Great M9.2 Alaska earthquake in 1964 (Davies & House, 1979; Plafker, 1965).

The Yakutat terrane has a lower seismic velocity than the rest of the Pacific plate; however, the *P* wave velocity is greater than 7 km/s at its base, implying that it was originally oceanic in nature (Christeson et al., 2010; Worthington et al., 2012). Receiver function studies show that at approximately 70 to 130 km depth, the subducted Yakutat material is approximately 20% slower than the surrounding mantle, with a thickness of 11–20 km (Ferris et al., 2003; Kim et al., 2014; Rondenay et al., 2008). These thickness estimates are supported by traveltime tomography that resolves a roughly 20 km thick LVL with *P* wave velocity below 8 km/s extending to 140 km depth (Eberhart-Phillips et al., 2006).

To model the guided wave arrivals accurately, the slab geometry must be known. Figure 1 compares the slab surface geometry from slab1.0 (Hayes et al., 2012) with the interface inferred from the receiver function profile to the west (Kim et al., 2014) and with the locations of Wadati-Benioff zone seismicity from various catalogs. The receiver function profile can be relied upon for the overall shape of the slab; however, much of the intermediate-depth seismicity plots above the two slab surfaces. We therefore infer the top of the slab directly from well-located earthquakes (with four or more depth phases) from the International Seismological Centre (International Seismological Centre, 2014) and Alaska Earthquake Information Centre catalogs (Alaska Earthquake Centre, 2016). The inferred surface of the slab is shown in Figure 1b.

3. Guided Wave Observations

Dispersed arrivals associated with guided wave propagation are observed at stations in the forearc along the Alaskan coast from the Anchorage area down to Kodiak Island. *P* wave dispersion is seen along the profile at broadband stations PWL, KNK, SAW, and GHO of the Alaska Regional Network from events up to 140 km depth. The positions of these stations relative to the trench are given in Figure 2a. We identify *P* wave dispersion by applying a Gaussian spectrogram to the vertical component following Abers (2000, 2005) and Garth and Rietbrock (2014a, 2014b, 2017). Dispersive events can appear as a gradual slope of increasing frequency with increasing time, but in this tectonic setting more commonly take the form of two distinct arrivals, low frequency and then high-frequency energy, with a delay of up to 4 s (see Figures 3a and 3c).

We selected 102 events for analysis from the Preliminary Determination of Epicenters (PDE) catalog, with depths greater than 40 km and moment magnitude above 3.8, that occurred on the profile shown in Figure 1 from 2012 to 2015. Of these events, 41 showed significant dispersion on at least one station. The clearest events with dispersion observed at multiple stations were selected for further analysis. The magnitude of time delay of high-frequency energy increases with source depth, due to increased time energy spends propagating through the LVL, as shown by waveforms from these events (Figure 2b).

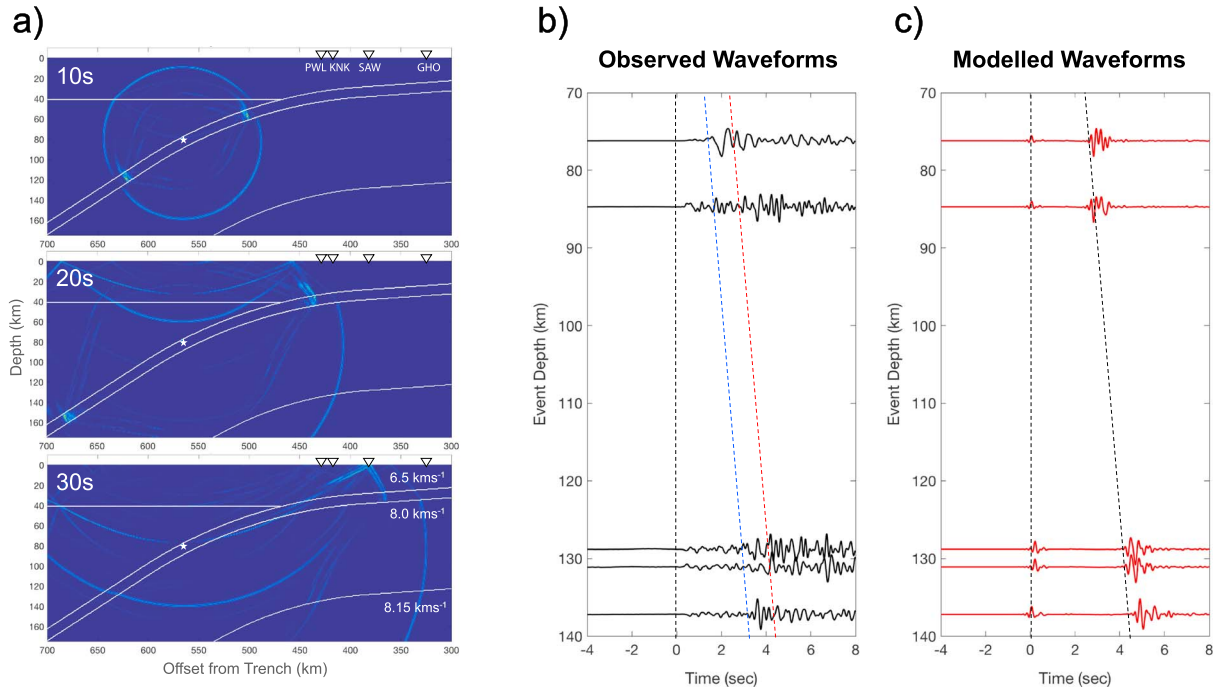

Figure 2. Synthetic and observed dispersed wave field. (a) Snapshots of the dispersive wave field at 10, 20, and 30 s after rupture. The velocity model is shown as white contours and dispersion observing stations as inverted triangles. (b) Waveform depth profile of low-pass filtered (<6 Hz) *z*-component data for events recorded at station KNK at various depths along the profile. (c) Synthetic waveforms for the same events. The dashed lines highlight the low-frequency first arrivals and the delayed high-frequency arrivals with an increase in delay time with depth. The red and blue dashed lines correspond to the delayed high-frequency arrivals for models with LVL *P* wave velocity 7.0 and 7.5 km/s, respectively.

4. Waveform Modeling of Guided Waves

We use 2-D full waveform modeling to simulate events within the LVL for a given velocity model. Using a grid search method, we vary *P* wave velocity and thickness parameters. Comparison of synthetic and observed waveforms then allows us to obtain the parameters that best fit the observed dispersion.

4.1. Model Setup

We produce synthetic waveforms using the 2-D finite difference waveform propagation code Sofi2D (Bohlen, 2002). The model is bounded with a free surface at the top and absorbing boundary conditions at the sides and base. A grid spacing of 75 m is used, producing synthetic waveforms accurate up to 5 Hz at the velocities considered. An explosive spike source excites *P* waves of all frequencies at a given hypocenter. Synthetic tests with a double-couple source, with fault plane angles likely for these subduction-related events, show that the results do not differ significantly from the explosive source simulations. All events used in analysis are smaller than Mw 5.0 to avoid source complexities.

The subducting slab and surrounding material are modeled as elastic media as attenuation in this subduction segment is relatively low (Stachnik et al., 2004), and it has been shown that small variations in attenuation have minimal effect on subduction zone guided wave dispersion (Garth & Rietbrock, 2014a). The seismic velocities in the slab model are informed by previous literature: the overlying crust is 40 km thick with velocity 6,500 m/s, and the continental mantle and slab mantle are 8,000 and 8,150 m/s, respectively (Eberhart-Phillips et al., 2006; Kim et al., 2014; Rondenay et al., 2008).

Hypocenter position and slab geometry have a large effect on the quality of dispersion observed at the surface. The PDE hypocenters used to identify potential events are relatively poorly constrained in depth compared to the resolution of the LVL structure. We therefore assume that if we see clear dispersion in the observations, the earthquake is favorably placed within the LVL (Martin & Rietbrock, 2006). This study and others (Garth & Rietbrock, 2014a, 2017) determine that clearest dispersion is seen when the source is placed in the top portion of the LVL (see Figure S1). Therefore, we place all sources at a depth of one fourth of the LVL

width from the top of the LVL. High-frequency energy decouples from the crustal layer either due to a bend in the slab (Martin et al., 2003) or equalization of seismic velocities between the LVL and overriding crust (Martin et al., 2005). While both decoupling mechanisms will contribute to the observed wave field, the numerical models suggest that the main mechanism seen in this subduction segment is the latter. Figure 2a shows snapshots of a numerical simulation of the dispersive wave field generated by an intermediate-depth source in the geometry inferred as in section 2.

Observational data and model results are analyzed and compared in both time and frequency domains. Both the waveform and velocity spectra for observations show complexity that could be caused by scattering structure not included in the models or by source complexity that is not reflected in the point sources implemented. Spectrograms are therefore used to provide the most meaningful quantitative comparison between model results and observational data. The model misfit to data is calculated by summing the difference in arrival time between the maximum amplitudes of the model and observation for each frequency band between 0.125 and 5 Hz.

4.2. Grid Searches

Finding a best fit model for the low-velocity crustal layer requires careful consideration of the trade-offs between LVL thickness and LVL *P* wave velocity. *P* wave velocity governs the magnitude of time delay between first and later arrivals, as well as the wavelength of the retained guided wave. LVL thickness affects the wavelengths that can travel through the waveguide. A thinner waveguide will only trap shorter wavelength, higher frequency waves, meaning a higher frequency band will be delayed in the spectrogram. This also affects the initial gradient of the curve in the spectrogram; a thinner LVL will produce a steeper first arrival in spectral space. Running a grid of models provides an effective way to simultaneously constrain LVL width and LVL *P* wave velocity.

Focusing on the clearest recorded event, at 84.7 km depth, we generate a grid of models for LVL width increments of 2 km between 4 and 20 km and LVL velocity increments of 0.2 km/s between 6.6 and 7.4 km/s, as shown in Figure 3b. Models with lowest misfit to data have LVL thickness 6–8 km and LVL *P* wave velocity 6.8–7.0 km/s. The spectrogram and waveform for one such model are shown in Figure 3a. To test this best fitting slab model, we implement a variety of source positions simulating four additional events and again compare the synthetic seismograms produced to observations for multiple stations. These comparisons are illustrated in the time domain for observations at station KNK in Figure 2b. As shown in Figure 2b the preferred velocity model fits most events well, only fitting the deepest event relatively poorly. Specifically, the time delay between low- and high-frequency arrivals for this 137.2 km deep event is shorter than for shallower events. To explore this anomaly further, we run a grid of models for this event, shown in Figure 3d. The best fitting results here give a LVL of thickness 8–10 km and *P* wave velocity 7.5–7.6 km/s (Figure 3c).

An increase in average *P* wave velocity within the LVL with depth is expected as oceanic crustal material is undergoing a series of metamorphic reactions; we therefore test models where the LVL to mantle velocity contrast reduces with depth, as in Garth and Rietbrock (2014a). However, because the average velocity increase is relatively large and occurs over a small distance in depth between the two modeled events, no physically reasonable variable velocity model produces a good fit to observations. An alternative solution to increase the average velocity experienced by the *P* waves traveling up from this deepest event is to assume that the subducted crust becomes fully eclogitized above the hypocenter. This would mean that energy would travel first through material of mantle velocity before becoming trapped in the LVL waveguide. To investigate this possibility, we test a suite of models with LVLs ending at various depths above the deepest event (see Figure S2). These velocity models either do not produce dispersion (if the LVL end depth is a large distance from the hypocenter) or do not significantly decrease the magnitude of time delay of the guided wave.

5. Discussion

The thickened Yakutat terrane has been inferred at depth beneath southern Alaska through a variety of seismic imaging techniques including receiver functions (Ferris et al., 2003; Kim et al., 2014; Rondenay et al., 2008) and seismic tomography (Eberhart-Phillips et al., 2006). Subduction zone guided waves spend longer interacting with the low-velocity structure of a subducted slab than any other seismic phase, and therefore

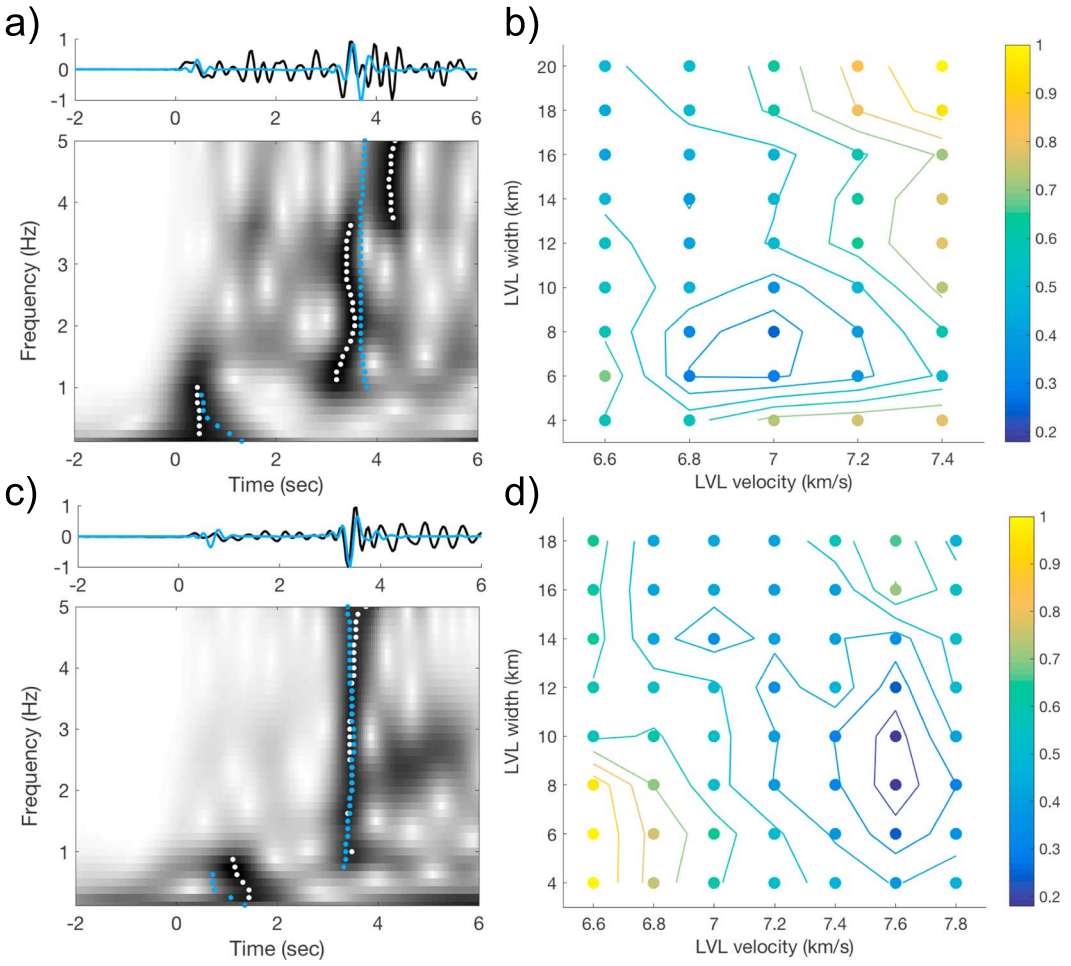

Figure 3. Best fit models compared to data, and grid search for observations on station KNK. (a and c) Waveforms and spectrograms for modeled events at 84.7 and 137.2 km depths, respectively. Observations given in black and white and maximum amplitudes of best fit model plotted in blue. (b and d) Grid searches to find best fitting thicknesses and velocities; the darker colors indicate lower normalized misfit. Best fit models are taken from grid search minima: 7.0 km/s *P* wave velocity, 8 km LVL thickness, and 7.5 km/s *P* wave velocity and 10 km LVL thickness.

have the potential to resolve previously unobserved details of the low-velocity structure. The 2-D numerical simulations of guided wave arrivals observed in the forearc of the eastern Alaskan-Aleutian subduction zone reported here give new constraints on the seismic velocity and width of the thickened subducting oceanic material.

Full waveform modeling suggests that the LVL is between 6 and10 km thick, and most events are accounted for by a LVL velocity of contrast of 12.5–15% with the overriding mantle material. The exception to this is a single event in the western corner of the Yakutat terrane that has a velocity contrast of 7–8%. These results suggest that the LVL is thicker and slower than suggested by previous guided wave studies that infer a range of thicknesses between 2 and 6 km (Abers, 2000, 2005; Abers & Sarker, 1996). This discrepancy is likely due to the along-strike raypath of the guided wave arrivals used in these previous studies, meaning that a composite of the thickened Yakutat terrane, and the thinner oceanic crust to the west, is sampled. The Yakutat terrane is widely accepted to be oceanic in origin with a mafic composition (e.g., Brocher et al., 1994; Christeson et al., 2010; Ferris et al., 2003). We therefore compare the velocities inferred from our guided wave constraints with predicted velocities expected for a range of mineral assemblages associated with metamorphosed mid-ocean ridge basalt (MORB) compositions, as shown in Figure 4a. The velocities are calculated for assemblages predicted to occur by Hacker et al. (2003) using the Excel macro of Hacker and Abers (2004) and the thermal model for the Alaskan subduction zone of Syracuse et al. (2010).

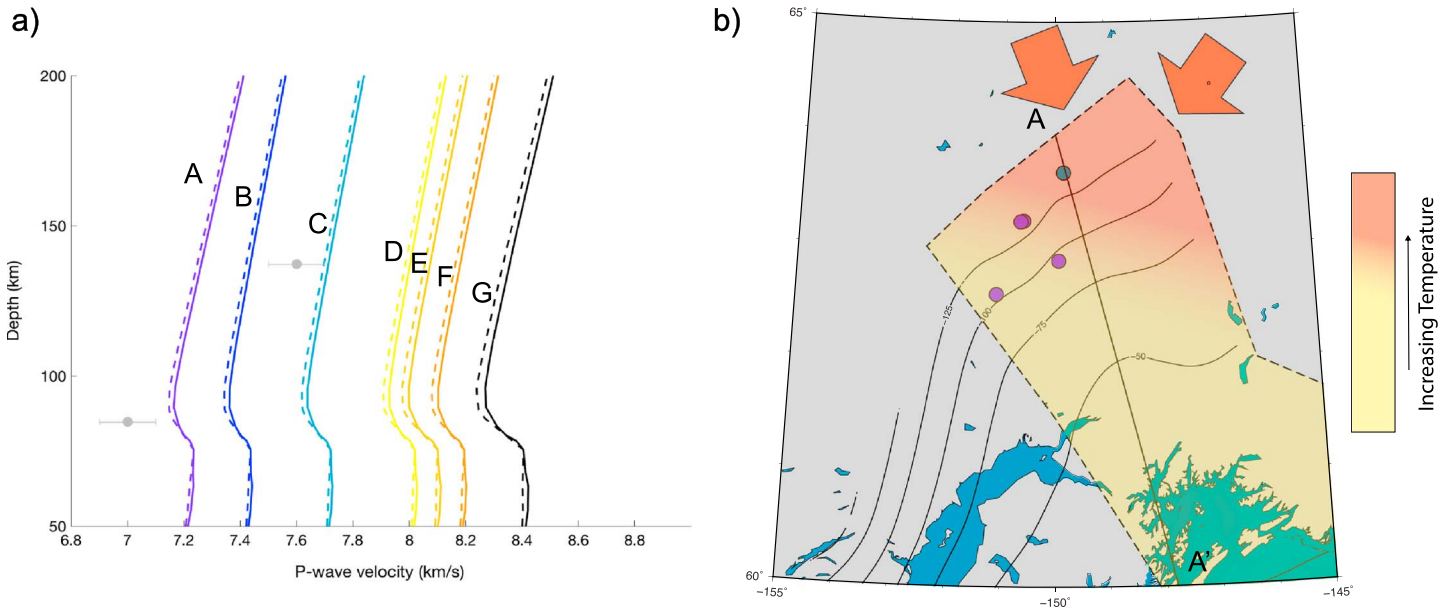

Figure 4. Summary of crustal velocities. (a) Comparison of MORB phase velocities with LVL velocities inferred for the subducted crust. Predicted velocities for the following MORB assemblages (a) lawsonite blueschist, (b) jadeite lawsonite blueschist, (c) lawsonite amphibole blueschist, (d) amphibole eclogite, (e) zoesite eclogite, (f) eclogite, and (g) pyrolite. Inferred velocities for the two modeled events are shown in grey. The dashed and solid lines represent the low-pressure and high-pressure bounds of the stability field. Velocities are calculated from the Excel macro of Hacker and Abers (2004) and thermal models of Syracuse et al. (2010). (b) Schematic summary of the proposed along strike variations close to the edge of the slab. The extent of the subducted Yakutat terrane is plotted as a black dashed line (Eberhart-Phillips et al., 2006). Events are colored by their closest inferred assemblages corresponding to a. Heating at the edge of the slab is illustrated by orange arrows, and a possible temperature gradient across the slab is given by a yellow to orange color gradient.

The faster LVL velocities inferred for the deepest event in the western corner of the Yakutat terrane are explained by the *P* wave velocities expected for uneclogitized metastable oceanic crust; the velocities correspond well with a lawsonite amphibole eclogite assemblage. The majority of events in the shallower and more westerly parts of the slab show a much slower *P* wave velocity, and therefore cannot be accounted for by expected metastable MORB assemblages alone.

Extensive testing has shown that the variation in *P* wave velocity between these events cannot be accounted for by gradational downdip increase in the velocity of the LVL, or by varying the depth at which the LVL transforms to higher velocity eclogite. To fit all modeled observations (shown in Figure 2b), we require a nonuniform transition in average velocity within the LVL. We propose that this variation in velocity is accounted for by a variation in conditions across the subducted Yakutat terrane. Lower velocities associated with the most westerly events show minimal variation from those observed in the unsubducted Yakutat terrane (Christeson et al., 2010). The presence of this metastable low-velocity structure may be due to anhydrous conditions in the lower part of the oceanic terrane (e.g., Chuang et al., 2017) or due to cooler temperatures here due insulation from the upper parts of the oceanic plateau. We hypothesize that the faster velocities seen from the event at the eastern edge of the Yakutat terrane may be caused by higher temperatures at the edge of the slab causing metamorphic reactions to occur more quickly in this part of the subducting crust. This is illustrated in Figure 4b.

The observations presented here generally suggest that at depth, the subducted Yakutat terrane is both thinner and faster than is inferred by receiver function studies in the area (e.g., Ferris et al., 2003). This discrepancy may, in part, be explained by the fact that the guided wave analysis is predominantly sensitive to *P* wave velocity structure, while the receiver function analysis is sensitive to gradients in both *P* and *S* wave structure. Recent seismic refraction studies of the presubducted Yakutat terrane at the trench show that it is at least 15 km thick with up to 9 km of overlying sedimentary layers entering the subduction zone at the surface (Christeson et al., 2010; Worthington et al., 2012). We reconcile these observations with our own result of a 6–10 km LVL at depth, by proposing that the seismically "visible" portion of the crust has been significantly thinned during subduction. Sediments atop the Yakutat terrane and the upper part of the terrane itself are

likely to have been accreted and underplated on to the overriding crust, while the upper parts of the oceanic material will metamorphose to eclogite, and so would no longer be seismically distinguishable from the surrounding mantle.

Based on the *S* wave velocity constraints from receiver function studies (e.g., Ferris et al., 2003) and the *P* wave velocity constraints presented here, we can infer the vp/vs ratio within the LVL to be 1.84–1.89. This is highly similar to the vp/vs ratio expected for mafic rocks (Brocher, 2005), suggesting that the LVL may be relatively anhydrous at this depth, impeding metamorphic reactions in this section of the subducted oceanic crust. This further supports the hypothesis that the LVL identified is a central core of the Yakutat terrane, where metamorphism is inhibited due to anhydrous conditions, and is in agreement with recent work suggesting that LVL imaged by detailed receiver function (e.g., Rondenay et al., 2010) corresponds to anhydrous gabbroitic lower crust that persists deeper than the more hydrated basaltic upper crust (Chuang et al., 2017).

6. Conclusions

Guided wave dispersion observed in this study is explained well by a single LVL, which is interpreted as the subducted Yakutat terrane. Our analysis gives a new constraint on the width of the LVL, indicating that it is 6 to 10 km thick, which is significantly thinner than previously suggested by receiver function studies. This inferred thickness implies that the Yakutat terrane has been thinned considerably during subduction. Guided wave observations are also extremely sensitive to the velocity of the subducted plate. Most of the observations can be explained by a LVL velocity of 6.8–7.0 km/s (12.5–15% slower than surrounding material). As these slower velocities cannot be fully accounted for by metamorphosed MORB or gabbro compositions, we propose that metamorphism is significantly inhibited in the shallower depth, southern portion of the subduction zone.

Anomalously fast velocities inferred from an event at the northernmost extent of the profile are modeled as metamorphosed gabbro or MORB assemblages, suggesting that slower velocity assemblages are no longer present in the deeper, northern part of the subducted Yakutat terrane. This may be explained by the warmer conditions at the edge of the subducted terrane causing a faster pace of metamorphic reactions in this part of the slab. Alternatively, the faster velocities inferred in this part of the subducted crust may be due to inherent heterogeneity in the subducted Yakutat terrane. These observations suggest that lawsonite bearing phases may persist in the lower part of the Yakutat terrane to depths of up to 140 km, well beyond the volcanic arc.

Acknowledgments
We thank Sean Gulick and Tom Brocher for their constructive reviews that greatly improved the final manuscript. Waveform data have been downloaded from IRIS data services. S. C. is supported by Frank Knox Memorial Fellowships and Harvard University.

References

Abers, G. A. (2000). Hydrated subducted crust at 100–250 km depth. *Earth and Planetary Science Letters*, *176*(3-4), 323–330. https://doi.org/10.1016/S0012-821X(00)00007-8

Abers, G. A. (2005). Seismic low-velocity layer at the top of subducting slabs: Observations, predictions, and systematics. *Physics of the Earth and Planetary Interiors*, *149*(1–2), 7–29. https://doi.org/10.1016/j.pepi.2004.10.002

Abers, G. A., & Sarker, G. (1996). Dispersion of regional body waves at 100–150 km depth beneath Alaska: In situ constraints on metamorphism of subducted crust. *Geophysical Research Letters*, *23*, 1171–1174. https://doi.org/10.1029/96GL00974

Alaska Earthquake Centre (2016). AEIC Earthquake Database.

Bohlen, T. (2002). Parallel 3-D viscoelastic finite difference seismic modelling. *Computers & Geosciences*, *28*(8), 887–899. https://doi.org/10.1016/S0098-3004(02)00006-7

Brocher, T. M. (2005). Empirical relations between elastic wavespeeds and density in the Earth's crust. *Bulletin of the Seismological Society of America*, *95*(6), 2081–2092. https://doi.org/10.1785/0120050077

Brocher, T. M., Fuis, G. S., Fisher, M. A., Plafker, G., Moses, M. J., Taber, J. J., & Christensen, N. I. (1994). Mapping the megathrust beneath the northern Gulf of Alaska using wide-angle seismic data. *Journal of Geophysical Research*, *99*, 11,663–11,685. https://doi.org/10.1029/94JB00111

Christeson, G. L., Gulick, S. P., van Avendonk, H. J., Worthington, L. L., Reece, R. S., & Pavlis, T. L. (2010). The Yakutat terrane: Dramatic change in crustal thickness across the transition fault, Alaska. *Geology*, *38*(10), 895–898. https://doi.org/10.1130/G31170.1

Chuang, L., Bostock, M., Wech, A., & Plourde, A. (2017). Plateau subduction, intraslab seismicity, and the Denali (Alaska) volcanic gap. *Geology*, *45*(7), 647–650. https://doi.org/10.1130/G38867.1

Davies, J. N., & House, L. (1979). Aleutian subduction zone seismicity, volcano-trench separation, and their relation to great thrust-type earthquakes. *Journal of Geophysical Research*, *84*, 4583–4591. https://doi.org/10.1029/JB084iB09p04583

Eberhart-Phillips, D., Christensen, D. H., Brocher, T. M., Hansen, R., Ruppert, N. A., Haeussler, P. J., & Abers, G. A. (2006). Imaging the transition from Aleutian subduction to Yakutat collision in central Alaska, with local earthquakes and active source data. *Journal of Geophysical Research*, *111*, B11303. https://doi.org/10.1029/2005JB004240

Ferris, A., Abers, G. A., Christensen, D. H., & Veenstra, E. (2003). High resolution image of the subducted Pacific (?) plate beneath central Alaska, 50–150 km depth. *Earth and Planetary Science Letters*, *214*(3-4), 575–588. https://doi.org/10.1016/S0012-821X(03)00403-5

Garth, T., & Rietbrock, A. (2014a). Downdip velocity changes in subducted oceanic crust beneath Northern Japan—Insights from guided waves. *Geophysical Journal International*, *198*(3), 1342–1358. https://doi.org/10.1093/gji/ggu206

Garth, T., & Rietbrock, A. (2014b). Order of magnitude increase in subducted H_2O due to hydrated normal faults within the Wadati-Benioff zone. *Geology*, *42*(3), 207–210. https://doi.org/10.1130/g34730.1

Garth, T., & Rietbrock, A. (2017). Constraining the hydration of the subducting Nazca plate beneath Northern Chile using subduction zone guided waves. *Earth and Planetary Science Letters*, *474*, 237–247. https://doi.org/10.1016/j.epsl.2017.06.041

Hacker, B. R., & Abers, G. A. (2004). Subduction Factory 3: An Excel worksheet and macro for calculating the densities, seismic wave speeds, and H_2O contents of minerals and rocks at pressure and temperature. *Geochemistry, Geophysics, Geosystems*, *5*, Q01005. https://doi.org/10.1029/2003GC000614

Hacker, B. R., Abers, G. A., & Peacock, S. M. (2003). Subduction factory—1. Theoretical mineralogy, densities, seismic wave speeds, and H_2O contents. *Journal of Geophysical Research*, *108*(B1), 2029. https://doi.org/10.1029/2001JB001127

Hayes, G. P., Wald, D. J., & Johnson, R. L. (2012). Slab1. 0: A three-dimensional model of global subduction zone geometries. *Journal of Geophysical Research*, *117*, B01302. https://doi.org/10.1029/2011JB008524

International Seismological Centre (2014). On-line Bulletin.

Kim, Y., Abers, G. A., Li, J., Christensen, D., Calkins, J., & Rondenay, S. (2014). Alaska Megathrust 2: Imaging the megathrust zone and Yakutat/Pacific plate interface in the Alaska subduction zone. *Journal of Geophysical Research. Solid Earth*, *119*, 1924–1941. https://doi.org/10.1002/2013JB010581

Kirby, S. H., Stein, S., Okal, E. A., & Rubie, D. C. (1996). Metastable mantle phase transformations and deep earthquakes in subducting oceanic lithosphere. *Reviews of Geophysics*, *34*, 261–306. https://doi.org/10.1029/96RG01050

Martin, S., Haberland, C., & Rietbrock, A. (2005). Forearc decoupling of guided waves in the Chile-Peru subduction zone. *Geophysical Research Letters*, *32*, L23309. https://doi.org/10.1029/2005GL024183

Martin, S., & Rietbrock, A. (2006). Guided waves at subduction zones: Dependencies on slab geometry, receiver locations and earthquake sources. *Geophysical Journal International*, *167*(2), 693–704. https://doi.org/10.1111/j.1365-246X.2006.02963.x

Martin, S., Rietbrock, A., Haberland, C., & Asch, G. (2003). Guided waves propagating in subducted oceanic crust. *Journal of Geophysical Research*, *108*(B11), 2536. https://doi.org/10.1029/2003JB002450

Plafker, G. (1965). Tectonic Deformation Associated with the 1964 Alaska Earthquake: The earthquake of 27 March 1964 resulted in observable crustal deformation of unprecedented areal extent. *Science*, *148*(3678), 1675–1687.

Rondenay, S., Abers, G. A., & Van Keken, P. E. (2008). Seismic imaging of subduction zone metamorphism. *Geology*, *36*(4), 275–278. https://doi.org/10.1130/G24112A.1

Rondenay, S., Montési, L. G., & Abers, G. A. (2010). New geophysical insight into the origin of the Denali volcanic gap. *Geophysical Journal International*, *182*(2), 613–630. https://doi.org/10.1111/j.1365-246X.2010.04659.x

Stachnik, J. C., Abers, G. A., & Christensen, D. H. (2004). Seismic attenuation and mantle wedge temperatures in the Alaska subduction zone. *Journal of Geophysical Research*, *109*, B10304. https://doi.org/10.1029/2004JB003018

Syracuse, E. M., van Keken, P. E., & Abers, G. A. (2010). The global range of subduction zone thermal models. *Physics of the Earth and Planetary Interiors*, *183*(1-2), 73–90. https://doi.org/10.1016/j.pepi.2010.02.004

Worthington, L. L., Van Avendonk, H. J., Gulick, S. P., Christeson, G. L., & Pavlis, T. L. (2012). Crustal structure of the Yakutat terrane and the evolution of subduction and collision in southern Alaska. *Journal of Geophysical Research*, *117*, B01102. https://doi.org/10.1029/2011JB008493